Progress Towards a Titanium-Zirconium-Molybdenum Alloy Coreblock Prototype Using Powder Bed Fusion

Michael J. Brand, Robin Montoya Pacheco, William P. Winter, Eric L. Tegtmeier,

and John S. Carpenter

Sigma Division: Metallurgy and Manufacturing Science

Los Alamos National Laboratory

LA-UR-22-29612

23 September 2022

Microreactor designs make use of a coreblock for structural stability allowing for these devices to provide powder generation while being portable and inherently safe. In order to maximize energy output of the microreactors, materials must be able to withstand high temperature without melting and without substantial decreases in mechanical properties. As simultaneous projects looking at steels, graphite, and other materials are on-going, this work package will investigate titanium – zirconium – molybdenum alloy (TZM) as it allows for potentially higher microreactor operating temperatures than traditional reactor materials such as stainless steel. Notably, this alloy was developed in the 1960s for use in rockets and has a very high melting point (2623°C) but is difficult to form, machine and join. With limited needs in aerospace, literature is appropriately sparce in looking at the AM of TZM (examples include [1,2]). However, the properties appear to be an excellent match for the needs of the microreactor coreblock leading to the current project. In addition, small washers form the bulk of TZM parts needed in aerospace while the microreactor community was looking at larger, more complex parts. Therefore, AM of TZM is being explored to enable near – net shape of components with the needed complexity to impact the nuclear energy field.

The brief amount of literature available shows that initial forays into the AM of TZM leads to materials with densities of 99.7% or so [2]. We have found in previous work at LANL that densities above 99.99% are needed to ensure adequate repeatability of mechanical properties [3]. Using LANL's techniques for process optimization, the aim is to produce AM TZM with densities that far exceed those seen in literature. As an example, our technique was able to move AM 304L stainless steel from 99.8% to 99.9995% density. This improvement in density enabled the improvement of the mechanical properties and greatly reduced their variability making the material suitable for load-critical engineering applications. We hypothesize that the same methodology, applied to AM TZM, can produce similar results.

In FY22 we initially targeted the initial development of process parameters for additively manufacturing TZM on our laser powder bed (LPB) additive manufacturing (AM) machine. Our hypothesis was that techniques used to densify AM stainless steel builds could be used to densify AM TZM builds. In order to test this hypothesis, we provided a project plan consisting of the following steps:

1) Procure and characterize available TZM feedstock. *Outcome:* Identify if commercially available powder is suitable for fabricating near fully dense AM material.
2) Perform single bead studies consisting of heat source (laser) interactions with TZM material. Characterize these using microscopy. *Outcome:* Identify the process window for creating stable TZM molten pools and inform step 3.
3) Perform density cube builds as informed by single bead studies. Characterize for porosity and test for mechanical properties. *Outcome*: Identify the optimal process parameters for seven hole block.

4) Build scaled seven hole prototype block out of AM TZM with optimal process parameters. *Outcome:* Identify any changes to process parameters necessitated due to geometric changes.
5) Fabricate test coupons out of AM TZM using optimal process conditions. *Outcome:* Have the samples on hand to build mechanical property data sets at both room and elevated temperatures in future years.

Our funding for this project was made available for charging at LANL in late May of 2022. Our initial plan called for steps 1 – 3 to be performed during FY22 and steps 3 – 5 to be performed during FY23. Despite ordering the powder on May 31st and an eight week delivery time, the powder has still not arrived from the vendor as of September 12th. This has led to a delay in performing step #3. This report, therefore, will focus on results from steps 1 and 2. Step 2, notably, is critical to overall success of the project. If success is not seen in step 2 (i.e. stable molten pools), then further progress towards steps 3 – 5 will not occur. As this report will show, our methodology, developed on stainless steel, appears to show a process window where the fabrication of AM TZM material is possible. This result reinforces the need to receive larger amounts of powder and to begin fabricating density cubes in FY23.

Feedstock Procurement and Characterization:

Purchase documents and quotes for substrate and powder production were assembled in May of FY22 with the purchase executed very soon after. The TZM base plates were received and have been machined to the appropriate size shown below. These plates will be used for two purposes.

1) The plates will be used to fabricate the single beads which will be used to determine the processing parameters for AM TZM, which will be discussed later in this report.
2) These plates will be used to fabricate parts i.e. density cubes and 7 hole coreblock during the first quarter of FY 2023.

Due to the cost of TZM, small base plates designed to fit into existing steel plates were purchased. This allows for the fabrication in steps 2 – 5 while keeping costs low, with the vast majority of the base plates (traditionally 300 mm x 300 mm x 125 mm) being out of stainless steel and only a small portion (seen in Figure 1) out of TZM. The preparation and machining of these plates was performed in LANL machine shops.

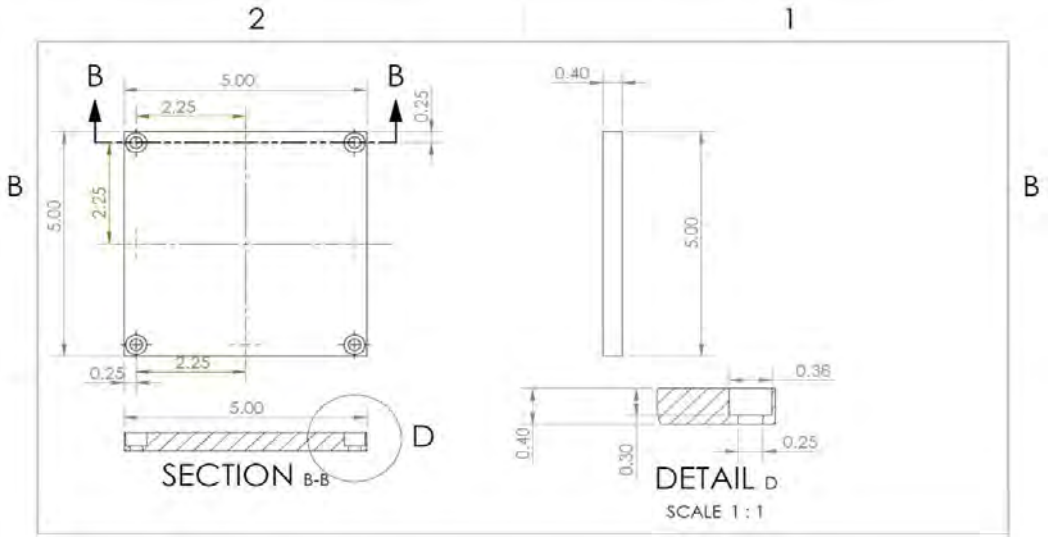

Figure 1: TZM build plates procured and machined this FY. Dimensions are in inches.

Procured Powder

Powder was ordered from HC Starck on May 31, 2022, in the quantity of 80Kgs. Due to shipping and receiving delays experienced this year, the powder is scheduled to arrive in mid-September 2022. However, in order to enable progress, LANL was able to secure a small sample of TZM powder from HC Starck in order for characterization to be performed.

The small amount of powder received was characterized at LANL to ensure that the powder was of sufficient quality to produce AM builds. In particular, the roundness, size, and porosity in the powder was investigated. Roundness of the powder impacts its spreadability which is critical to creating the thin layers of powder (60 um ± 5 um) evenly across the 300mm x 300mm build surface. Size distribution is also critical powder that is too large cannot be spread accurately in the thickness required. Porosity in AM builds stems primarily from two reasons; 1) Process parameters are inadequate and lead to areas that are short in powder or power leading to lack-of-fusion (LOF defects) and 2) Gas trapped porosity from within the powder particles that is carried through the process. The gas trapped porosity floats within the molten pool during AM and can solidify as a porous defect in the final microstructure. The first cause of porosity arises as a result of the inherent powder quality and process parameters. The second cause of porosity arises as a result of the inherent powder quality. In this portion of the project, the inherent quality of the powder and its fitness for use in our additive manufacturing system was explored.

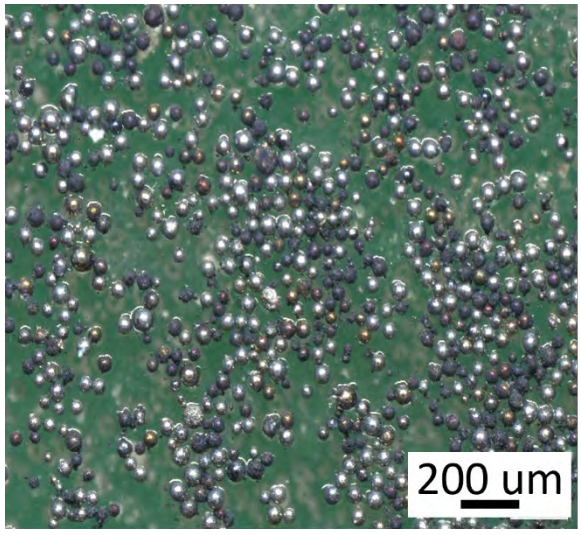

Figure 2: Optical photos of TZM powder showing round powder particles ideal for spreading in an AM system.

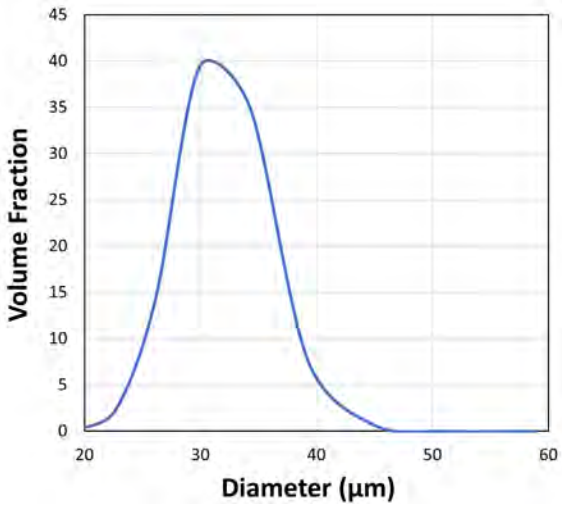

Figure 3: Results of size distribution study for incoming TZM powder. Cut size shows perfect distribution for use in upcoming AM builds.

Figure 2 shows a representative image of the powder. These optical images show powder particles with consistently round shapes ideal for spreading in additive manufacturing systems. Jagged particles can jam the system and lead to build failures. General images were taken to show the overall shape of the powder. Looking at the images below the powder is spherical and round which will help when building parts because there will be a clean, consistent spread across the build plate, ensuring that parts being built will have a uniform distribution of powder spread for each layer of the build.

Particle size analysis was performed on the powder. The resulting plot in Figure 3 shows the distribution of the particles. The powder had an average size of 30µm and had a range of 15µm-45µm. This is what is needed for optimum performance of the spreading action within the AM system used in this study.

A representative amount of individual powder particles were characterized using a Plasma Focused Ion Bean electron microscope (PFIB) at LANL. Using the plasma focused ion beam, powder particles underwent serial sectioning to look for hidden porosity defects within individual powder particles. These pores are often transitioned into the solidified, built material because of the rapid cooling rate seen in powder bed additive manufacturing. Images from this study are shown in Figure 4. Figure 4b shows the largest pore seen within the sectioned powder particles. The study indicated that the powder was of high quality with porous defects appearing fewer times and in smaller sizes than that observed in stainless steel powder used to make high density AM parts [3,4].

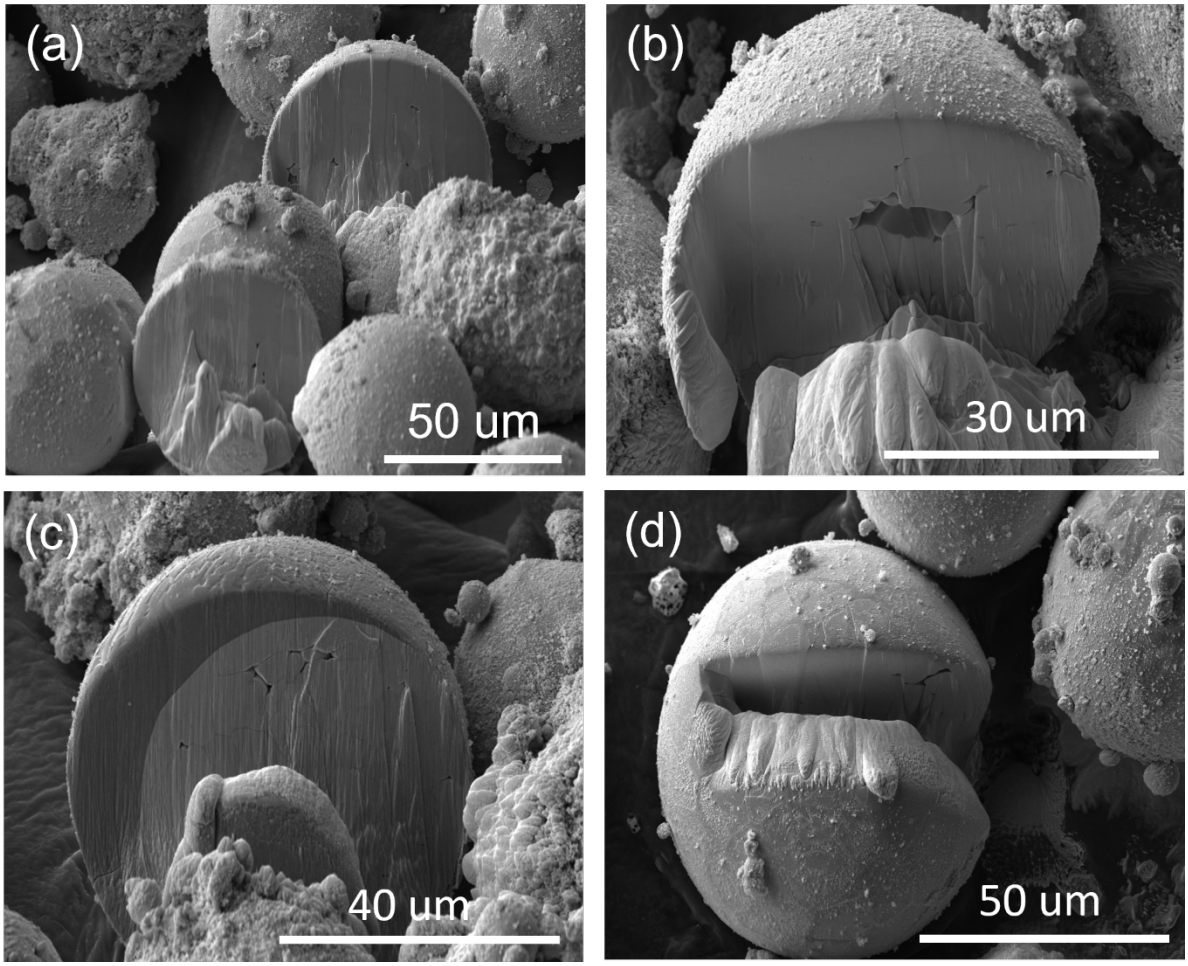

Figure 4: Individual powder particles imaged using PFIB. Powder exhibits very little porosity as compared to material used in the past.

Process Development through Single Bead Studies

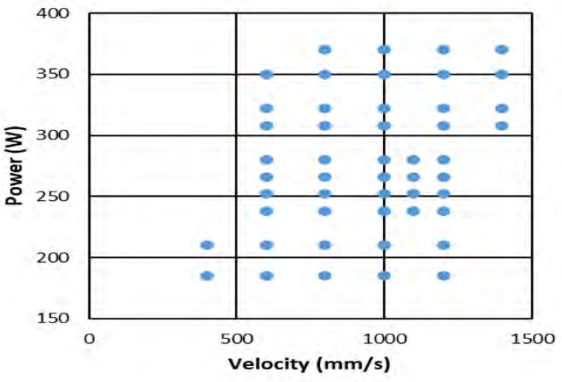

Figure 5: Power and Velocity Combinations tested for single beads

Experiments were performed using an EOS M290 Laser Powder Bed system using no powder on TZM plates described earlier and shown in Figure 1. A test matrix of various laser power and laser velocity combinations was created, which is shown in Figure 5. The melt pool optimization was performed where 49 combinations of laser power and scan speed were selected. Ten 10 mm long single-bead scans were rastered onto the build plate for each condition. Each set of single-beads were then cut in half and the welds were viewed

using an optical microscope [5-7]. The combinations were selected to span the operating region of the EOS M290. The single bead testes were laid out as shown in Figure 6, with forty-nine different configurations that varied only velocity and power. There are ten different scans for each group to give statistical repeatability when looking at the individual beads. These tests were performed using no powder consistent with published methodology to reduce overall cost

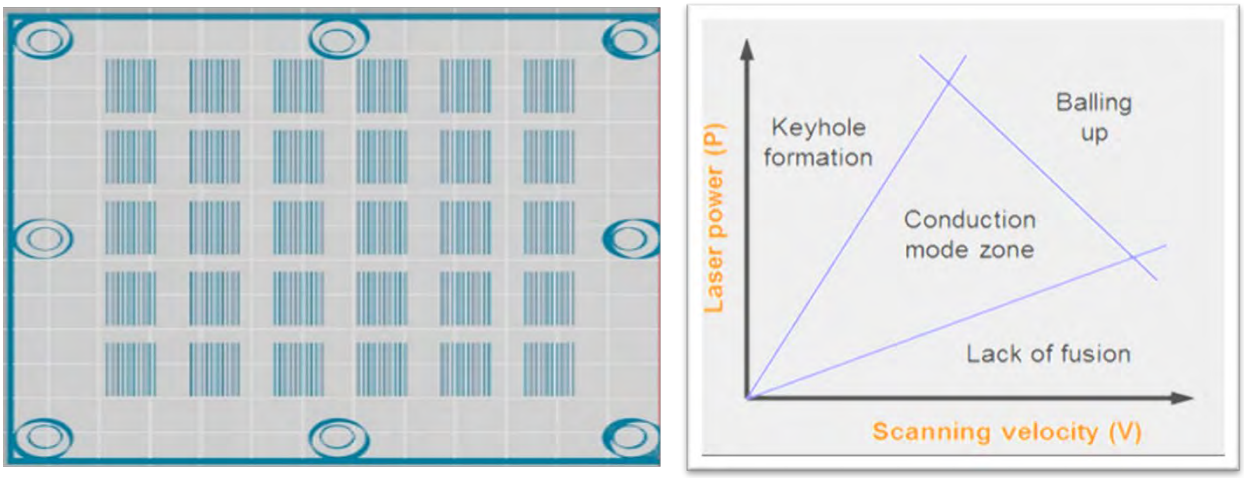

Figure 6: Image on left shows representation of beads placed on TZM plate with varying laser powers and laser velocities. For scaling information, please see Figure 1. On the right shows a representation of target weld profiles that are expected to be observed [8].

(TZM powder is expensive) and to provide an upper limit as the complete lack of powder represents the 'worst case scenario' for material-heat source interactions. The tests were performed to emulate the exact machine set up conditions and atmosphere that would be used when powder is introduced. The goal is to study the geometries of the welds that are produced when doing a single laser scan on a TZM plate. Figure 7 shows an example of a weld geometry and what is being looked at when the single beads are sectioned. Figure 7 shows what the ideal weld that would be required when looking at the single track/bead images. A width that is about 80µm and a depth of about 80µm which is about 2-3 times the layer thickness (30µm). Achieving a weld bead with these dimensions in AM TZM would constitute a successful result and make step 3 possible. Critically, The optimal results will likely sit in the conduction mode zone. The purpose of the single bead study is to identify the boundaries shown in Figure 6 and quantify where and if a conduction mode zone is possible for AM TZM. Obtaining solidified weld pools similar to

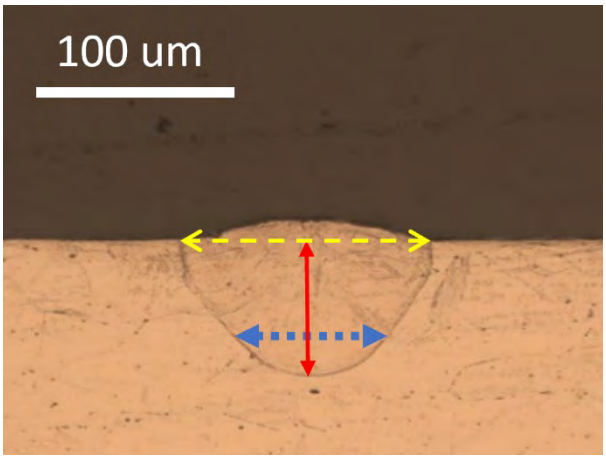

Figure 7: Example of a 316L weld bead and areas of interest
Width = Yellow Width @ 80µm
Depth = Blue
Depth = Red@80µm

that seen in Figure 7 would provide a strong indication that conduction mode had been achieved within the AM system.

Notional power-velocity collected in this study is illustrated in Figure 8 representing a significant leap for AM TZM development. Note that a conduction mode is present but is far narrower than that seen in most steels and common AM materials (see Figure 6). Understandably, the high melting temperature of TZM leads to a wide band of undermelting (marked in yellow) in Figure 8. In these cases, despite high laser speeds, insufficient power was presented to the material to create an optimized molten pool. On the opposite hand, high power coupled with lower laser velocities lead to keyhole mode welding and the creation of unstable molten pools with significant porosity. Although the band of conduction mode welding is smaller than in other materials, this is sufficiently wide enough to explore the impact of process parameters on mechanical behavior and porosity in step 3 in FY23.

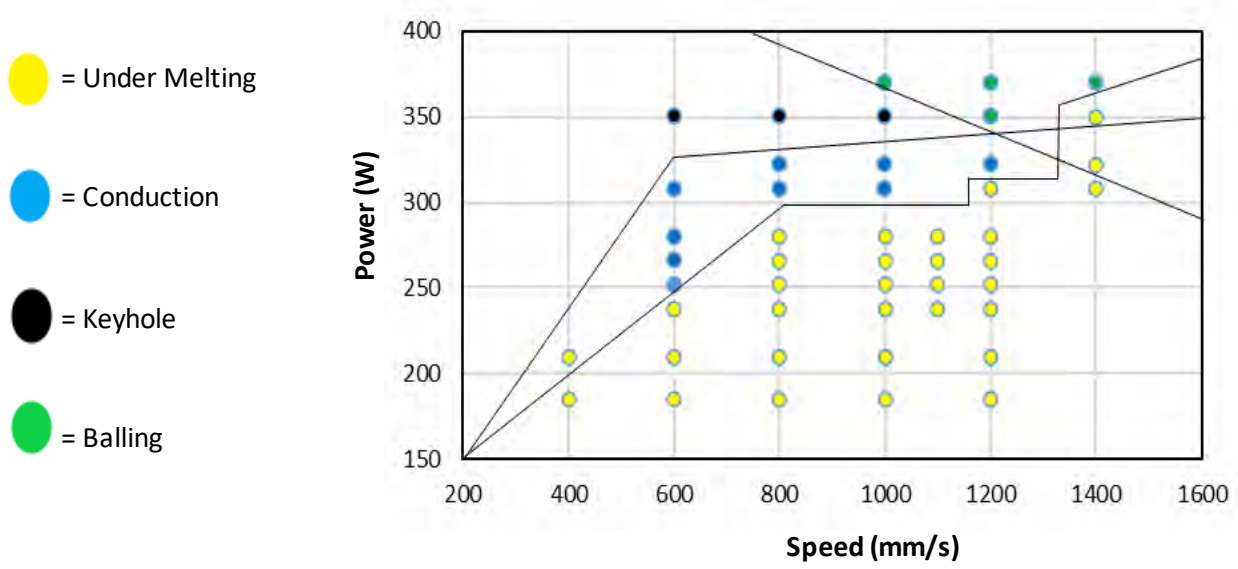

Figure 8: Experimentally – derived P-V map illustrating different melting modes captured in AM TZM. Note that conduction mode welding using current AM system was found for a variety of laser power – laser velocity combinations. This is promising for the density cube study (step 3) to be conducted in FY23 after the arrival of new powder.

Figure 9 shows the distribution of welds that have been studied for 4340 Steel. In many cases, it is observed that there are sharp distinctions in the weld geometries described in Figure 6. Balling is clearly shown in the upper right (high V / high P) and keyhole mode welding (low V / high P) is shown in the lower left. Note that conduction mode with optimal geometry is seen in the middle with symmetric molten pools that have the right aspect ratio (depth to width). Undermelting is clearly seen in the upper left where combinations of low P coupled with high V lead to inadequate melting. Figure 9 represents an effort to develop process parameters for a new type of steel for AM that was performed at LANL in conjunction with Worcester Polytechnic Institute covered in [2]. Figure 10 shows the distribution of the welds for the TZM single beads captured in this project. It shows the different types of welds that were received which are similar to the welds that were studied under the 4340-steel project.

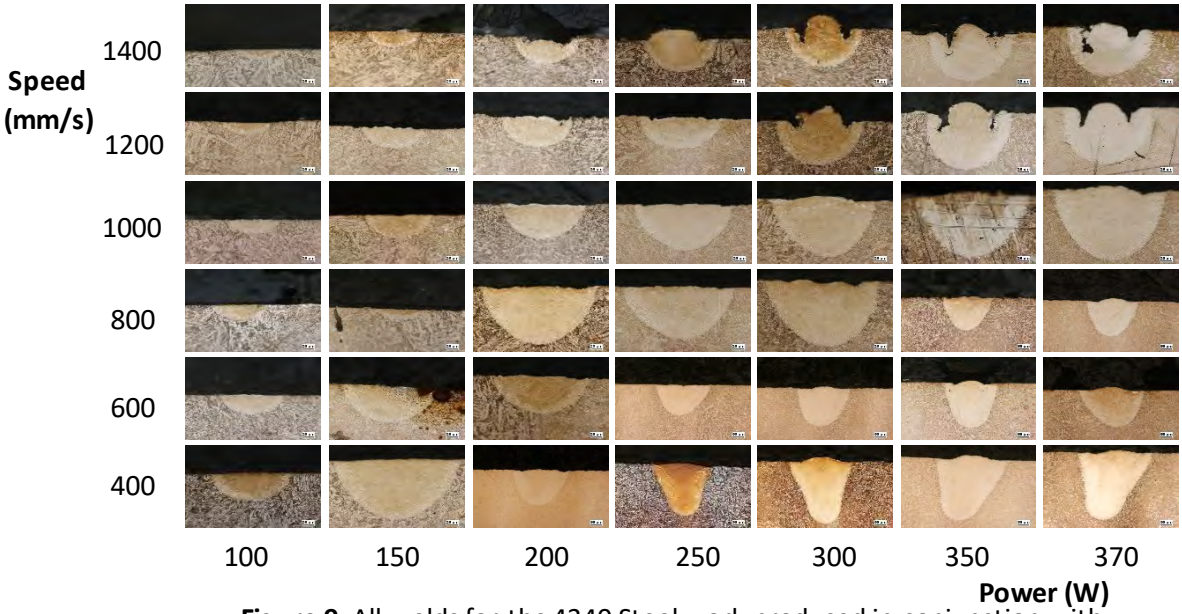

Figure 9: All welds for the 4340 Steel work produced in conjunction with Worcester Polytechnic Institute [5].

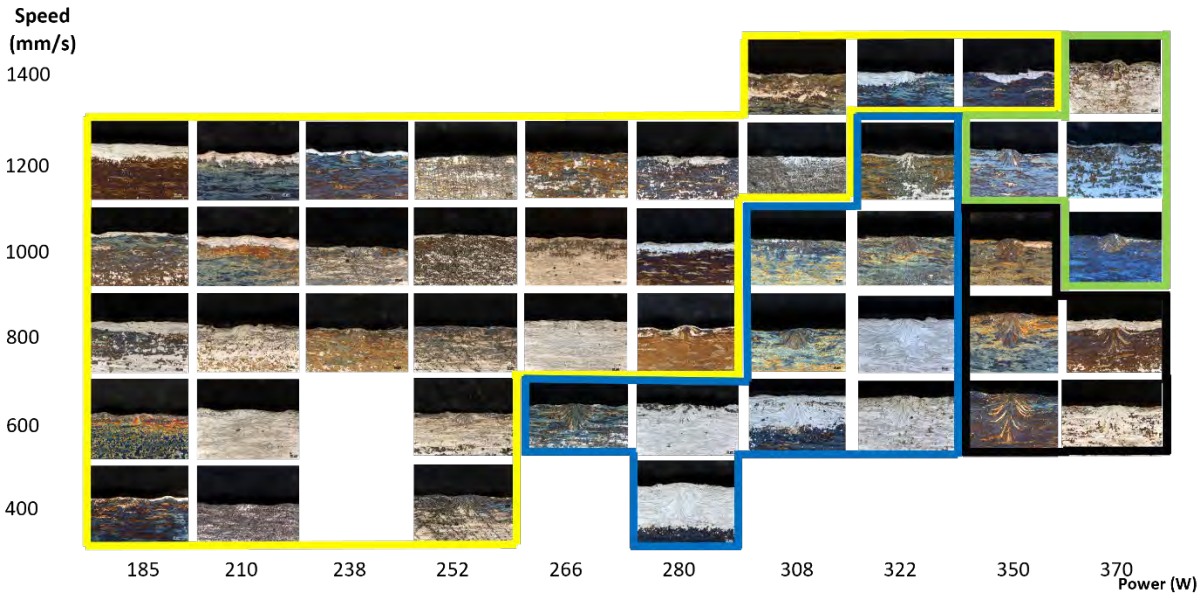

Figure 10: Process parameter development for AM TZM. Note that area captured in the blue box represents conduction mode welding and processing conditions with enough promise to further study in FY23.

As seen in Figure 10, all regions of the P-V map were discovered during this AM TZM study. The majority of the combinations tested show a lack of fusion marked in the yellow box in Figure 10. This makes sense because, compositionally, 99% of the material is Molybdenum based which has a higher melting temperature thus requiring higher power from the machine. There are ten combinations that are in the middle or conduction mode zone that show good to great weld geometry. These ten samples will then be used when powder is introduced to create density cubes that will be sectioned and viewed under a microscope. Images below show the different modes that are represented on the P-V map. Figure 11 provides two examples of weld pools consistent with undermelting. Note that in some cases, penetration is less than 10 um deep pointing to significant problems in building layers of 30 um or larger.

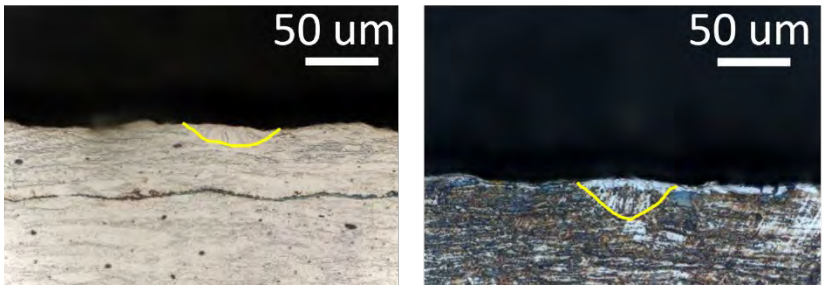

Figure 11: Two examples of undermelting observed in the section marked in yellow in Figure 10. Penetration is inadequate and aspect ratio is incorrect for stable molten pools and the use of these P-V combinations for dense AM builds.

Figure 11 represents under-melting. If these P-V combinations were to be used when fabricating density cubes, then there would be a severe amount of porosity present in the samples. The samples would not build at the predicted rate causing problems with the machine during fabrication, e.g. a recoater jam. These parameter sets would also produce a significant amount of spatter. Spatter is when powder and other process artifacts are ejected from the molten pool leading to porosity and potential machine malfunctions compromising the part. The combinations range from low power / low speed to high power / high speed as seen in Figure 10.

Figures 12 show a weld that would be ideal to use when fabricating density cubes. This weld look similar to that in Figure 7.

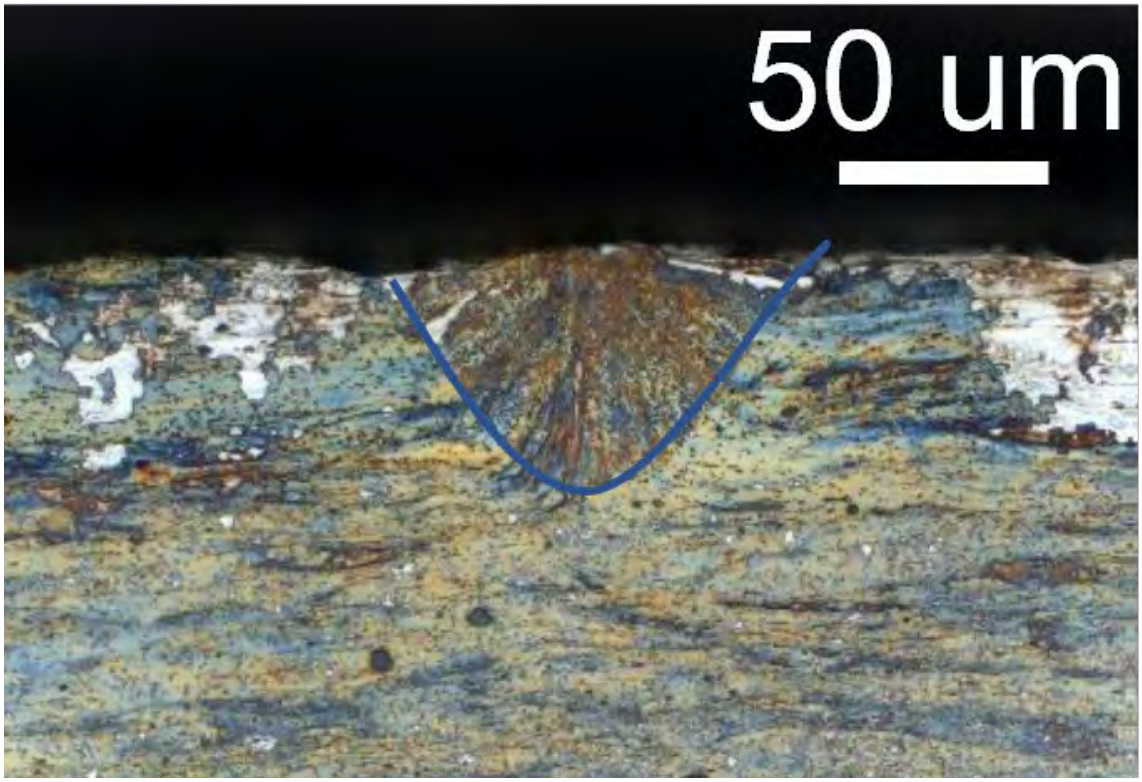

Figure 12: Conduction mode weld bead observed in AM TZM. It shows adequate depth, width and repeatability to allow for use in the fabrication of density cubes.

This P-V (322 watts ; 1000 mm/sec) combination would exhibit very high density and low porosity. Several combinations exist showing that intermediate speed coupled with high power can effectively build AM TZM. This is a promising result and allows the fabrication of density cubes in FY23. Another example of a strong conduction mode molten pool can be observed in Figure 13.

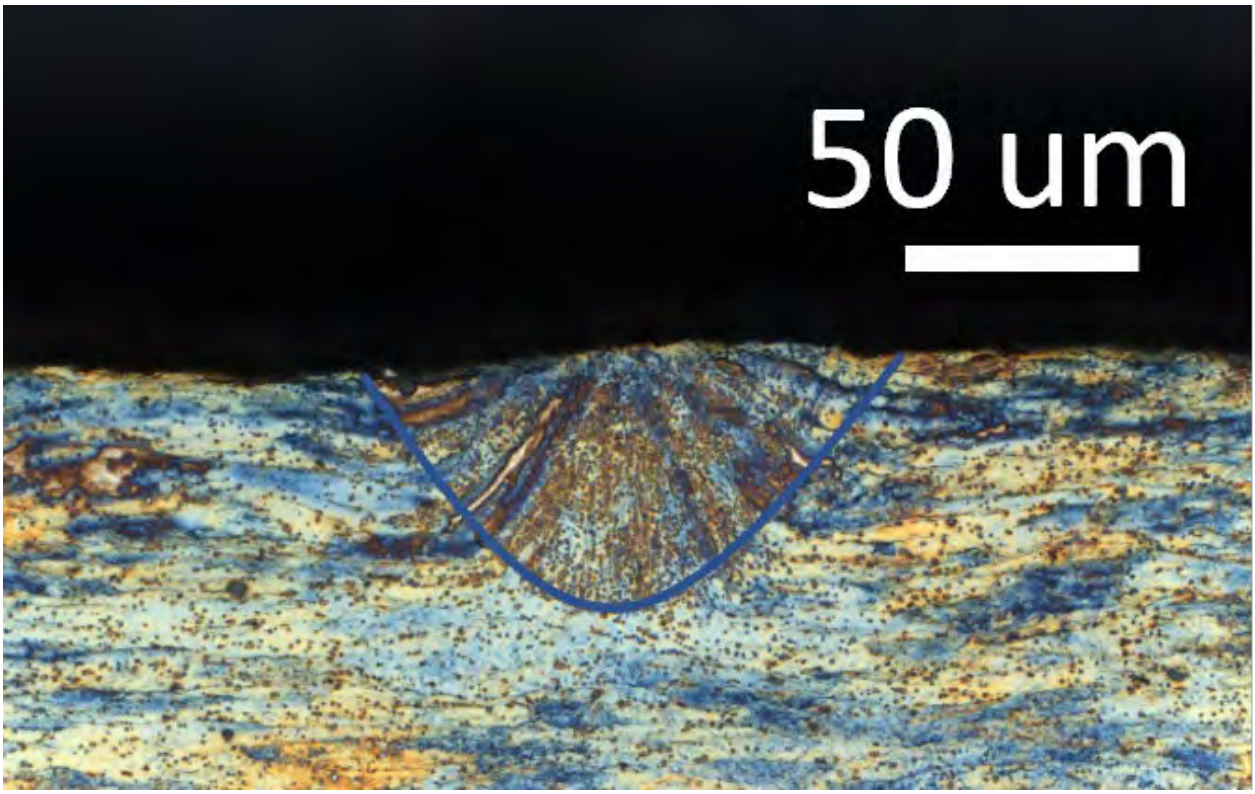

Figure 13: Conduction mode weld bead observed at 308 Watts with 800 mm/sec laser velocity.

These results show unequivocally that the heat source encompassed within the AM build can melt TZM and create predictable, repeatable molten pools consistent with large scale builds.

Figure 10 also shows results of balling and keyhole mode weld pools in green and black, respectively. In Figure 14, the cross-section associated with balling is made clear with the green line. Note that some penetration occurs. However, the molten pool does not reach a stable smooth shape prior to solidification indicating that the cooling rate was too rapid and that laser speed needs to be slowed down. This result would undoubtedly cause build failures as smoothing a layer of powder over a 'balled' or rough surface would lead to cascading build errors.

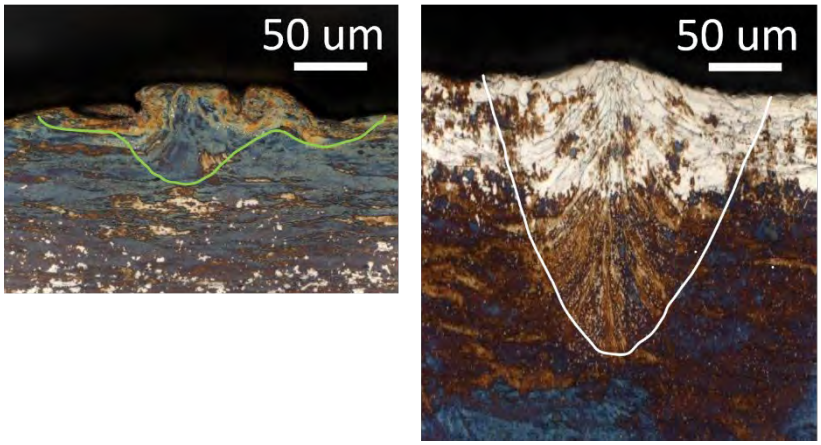

Figure 14: Balled and keyhole mode weld beads are shown for AM TZM. Neither morphology is appropriate for future study.

Likewise, Figure 14 also shows a keyhole mode weld bead. It is marked with a white, as opposed to black, line for clarity. Note that the penetration depth would lead to re-melt of a large number of layers (each layer being ~30 um thick). In this case, the laser velocity is too slow and laser power is too high leading to energy inputs that lead to this type of morphology. This should be avoided as keyhole mode welds can often lead to entrained porosity (not seen in Figure 14). In addition, the heat input could potentially lead to large amounts of distortion. Distortion in the z or build direction often leads to recoater jamming during spreading. Distortion in x and y directions (perpendicular to the build direction) often lead surface roughness and cracking.

Conclusion

TZM has historic use in property-critical, high strength, and high temperature applications in aerospace. In this project, the exploration of TZM as a material for use in microreactors was explored from the perspective of manufacturability. Microreactor coreblocks require precise and complex dimensioning which has been met in the past by AM stainless steel. In order to increase the energy output and efficiency, lessons learned from previous studies on AM stainless steel were employed to help mature the AM process for TZM. It was found that, despite the much higher melting temperature, the AM machines were capable of melting TZM and creating predictable and repeatable molten pools. The trends shown in Figure 10 clearly show a band of producibility for this material which will be used in FY23 to explore the impact of process parameters on density and mechanical behavior. The expectation is that low porosity AM TZM is well within the realm of possibility once TZM powder feedstock arrives.

References

[1] J.H. Vanhoose, "Investigating Using Titanium Zirconium Molybdenum for Additively Manufacturing Aerospace Components" (2019). *Open Access Theses & Dissertations*. 2017. https://scholarworks.utep.edu/open_etd/2017

[2] L. Kaserer, J. Braun, J. Stajkovic, K.-H. Leitz, P. Singer, I. Letofsky-Papst, H. Kestler, G. Leichtfried, "Microstructure and mechanical properties of molybdenum-titanium-zirconium-carbon alloy TZM processed via laser powder-bed fusion", International Journal of Refractory Metals and Hard Materials, Volume 93, 2020, 105369, ISSN 0263-4368.

[3] J.S. Carpenter, C.W. San Marchi, D.K. Balch, B.A. Meyer, et al. "Increasing the Readiness Levels of Additively Manufactured Reservoirs: Report on FY20 Activities," LA-CP-20-20601 (2020).

[4] B.M. Morrow, T.J. Lienert, M.J. Brand, et al. "Impact of Defects in Powder Feedstock Materials on Microstructure of 304L and 316L Stainless Steel Produced by Additive Manufacturing." *Metall Mater Trans A*, 49, (2018), p. 3637-3650.

[5] M.A. Ryder, C.J. Montgomery, M.J. Brand, et al. "Melt Pool and Heat Treatment Optimization for the Fabrication of High-Strength and High-Toughness Additively Manufactured 4340 Steel." *J. of Materi Eng and Perform* 30, (2021), p. 5426–5440.

[6] X. Shi, S. Ma, C. Liu and Q. Wu, "Parameter Optimization for Ti-47Al-2Cr-2Nb in Selective Laser Melting Based on Geometric Characteristics of Single Scan Tracks." *Opt. Laser Technol.*, 90, (2017), p 71–79.

[7] Y. He, C. Montgomery, J. Beuth and B. Webler, "Melt Pool Geometry and Microstructure of Ti6Al4V with B Additions Processed by Selective Laser Melting Additive Manufacturing." *Mater. Des.*, 183, (2019), p 108126.

[8] J. Beuth, et al. "Process mapping for qualification across multiple direct metal additive manufacturing processes." *2013 International Solid Freeform Fabrication Symposium*. University of Texas at Austin, 2013.